Forest Volume Estimation Method Based on Allometric Growth Model and Multisource Remote Sensing Data

Yanjie Wu, Zhihui Mao, Lijie Guo, Chenrui Li, and Lei Deng

***Abstract*—The accurate forest volume is crucial for forest management, but rapid, large-scale, and high-accuracy estimation is still challenging. We proposed a method of coupling allometric growth model and multisource data for forest volume estimation (CAMFVe). First, the diameter at breast height (DBH) estimation model is constructed by terrestrial laser scanning (TLS) and airborne laser scanning (ALS) to obtain more accurate measured volume. Second, the spectral attributes of Landsat and structural attributes of ALS are extracted and upscaled onto the 30-m plot scale, and the optimal attributes for volume estimation are selected. Third, the model of CAMFVe is constructed and applied to obtain the volume of study area. Finally, the applicability of CAMFVe is evaluated under four forest growth environments (different canopy closure and slope categories), and the accuracy is compared with multiple linear regression (MLR), random forest (RF), and support vector machine (SVM). The results show the following. First, the DBH estimation model by TLS and ALS improves the DBH calculation accuracy of ALS with a 2.058 cm reduction in RMSE. Second, the mean of canopy height (H_{mean}) and enhanced vegetation index (EVI) are identified as the optimal structural and spectral attributes, respectively. Third, the model constructed by H_{mean} and EVI consistently achieves higher accuracy for most forest growth environments, and the addition of spectral attribute improves volume estimation accuracy with a 10.152% reduction in RMSE compared with the H_{mean}-based model. Fourth, compared with MLR, RF, and SVM, CAMFVe offers higher accuracy, requires fewer parameters, and is simpler and more efficient. Our proposed method, based on allometric growth model and utilizing vegetation index instead of DBH, provides a solution for large-scale and high-accuracy volume estimation by combining spaceborne light detection and ranging and optical satellite images.**

***Index Terms*—Allometric growth model, forest volume, tree height, UAV light detection and ranging (LiDAR), vegetation index (VI).**

Manuscript received 19 June 2023; revised 19 August 2023; accepted 4 September 2023. Date of publication 8 September 2023; date of current version 2 October 2023. This work was supported by the R&D Program of Beijing Municipal Education Commission under Grant KZ202210028045. *(Corresponding author: Lei Deng.)*

Yanjie Wu, Lijie Guo, Chenrui Li, and Lei Deng are with the College of Resource Environment and Tourism, Capital Normal University, Beijing 100048, China (e-mail: 2210902132@cnu.edu.cn; 2210901025@cnu.edu.cn; 2210902101@cnu.edu.cn; denglei@cnu.edu.cn).

Zhihui Mao is with the College of Resource Environment and Tourism, Capital Normal University, Beijing 100048, China, and also with Resource and Environment Research Center, Chinese Academy of Fish Sciences, Beijing 100048, China (e-mail: mzhihui0506@163.com).

Digital Object Identifier 10.1109/JSTARS.2023.3313251

I. Introduction

FORESTS are the largest carbon pool in terrestrial ecosystems, and fully exploiting the carbon sequestration potential of forests is crucial to the improvement of human ecological environment and sustainable economic development [1], [2]. Forest volume is the basic data source for biomass and carbon sink estimation [3], [4]. Large-scale and high-accuracy estimation of forest volume is a prerequisite for improving forest quality and maximizing forest ecosystem functions and carbon sequestration potential. It is of great significance to forest management, carbon balance, and ecosystem monitoring research [5], [6]. Traditionally, forest volume is obtained by direct harvesting or allometric growth model, such as the volume table method [7], [8]. The direct harvesting method has high accuracy, but it is destructive and not suitable for large-scale spatial continuous volume estimation [9]. The allometric growth model method is to establish a regression equation with physical meaning between the volume obtained by harvesting and the stand characteristics, such as diameter at breast height (DBH) and tree height (H), obtained by artificial ground measurement, and then input the stand characteristics, such as DBH and H, into the equation to obtain the volume [10]. Especially, the allometric growth model constructed by DBH and H has high accuracy ($R^2 > 0.9$) and is widely used [11]. However, the acquisition of DBH and H is time-consuming and laborious, making it difficult to obtain the spatial distribution and dynamic change of large area forest resources timely and accurately [12], [13]. How to realize large-scale and high-accuracy forest volume estimation is an active field of research.

Over the past 30 years, the rapid development of remote sensing and information technology has made it possible to dynamically and accurately monitor forest resources and quickly map large areas. The existing studies have attempted to estimate large-scale forest volume through different remote sensing data and modeling methods [14], [15], [16]. Optical remote sensing generally establishes a regression model between the measured forest volume and remote sensing indices, such as normalized difference vegetation index (NDVI) and enhanced vegetation index (EVI) to provide a spatially continuous forest volume by analyzing the pixel brightness value of satellite images [17], [18], [19]. However, depending on the forest growth environments, the estimation accuracy may be limited to 10%–50% [20] and may be affected by saturation effects [21]. Although

optical images can capture the spectral heterogeneity of forest stands composed of different species, they cannot penetrate the canopy and, therefore, cannot provide information on the vertical structure of the forest. This may result in high estimation uncertainty in dense and multilayer canopy areas [22], [23].

Light detection and ranging (LiDAR) is an active remote sensing technology that has developed rapidly over the past decade. It can obtain both horizontal and vertical structure information of forests at the same time, and the obtained point cloud can be used to accurately estimate tree height, DBH, crown diameter (CD), and other structural attributes [24], [25]. LiDAR-derived structural attributes (H, DBH, etc.) can be combined with allometric growth models to achieve high-accuracy forest volume calculation in a certain range or used in conjunction with field measurements to estimate forest volume through regression models with higher accuracy than optical remote sensing [26]. Airborne laser scanners (ALS) can obtain H with high accuracy [27]. However, due to the limitations of echo frequency and intensity, it is difficult for LiDAR to penetrate the canopy to obtain tree trunk point clouds in areas with dense forest canopy. As a result, the accurate DBH information cannot be obtained [28]. Terrestrial laser scanners (TLS) have been proven to be an effective way to obtain high-accuracy DBH [29], [30] with an error not exceeding 1 cm, but the accuracy of H needs to be improved. The feature-level fusion of ALS and TLS may be able to achieve high-precision forest volume calculation within a certain range. However, due to the high level of automation, precision of instruments, and high cost of data acquisition in LiDAR, the acquisition of ALS and TLS data is still limited by the spatial extent and it is difficult to achieve large-scale regional coverage or high-frequency access [31]. The existing spaceborne LiDAR systems, such as the global ecosystem dynamics investigation (GEDI) onboard the international space station [32] and the advanced topographic laser altimeter system onboard the ice, cloud, and land elevation satellite-2 (ICESat-2) [33], can acquire a wide range of height-related data without the limitation of spatial extent, but DBH data are still not widely available. Moreover, due to the inability of lasers to obtain spectral information of vegetation, LiDAR has low accuracy in distinguishing and classifying tree species [30], [34].

To further improve the estimation accuracy of forest volume, collaborative modeling of optical images and LiDAR has been proposed [35], [36], [37], which can provide both spectral and structural information, thus improving the volume estimation accuracy. For example, the authors in [35] and [38] found that the fusion of optical images and LiDAR can improve the accuracy of forest volume estimation by 5%–20%. However, the existing studies simply input them into regression models, such as multiple linear regression (MLR), random forest (RF), and support vector machine (SVM) [35], [37], [39]. These machine learning methods have complex principles and typically require a large amount of field measurement data and multiple variables to establish the corresponding relationship between volume and various variables. Moreover, feeding more variables into the regression model may lead to collinearity problems and does not necessarily improve accuracy [40].

In summary, the allometric growth models constructed by DBH and H have high accuracy, but DBH and H are difficult to obtain in a large range. Spaceborne LiDAR systems, such as GEDI and ICESat-2, have made height-related attributes easier to obtain, but DBH is still difficult to obtain on a large scale [41], [42]. DBH, in essence, is an attribute representing the constant and irreversible characteristics of tree growth, and it is related to the metabolic rate of trees [43]. The spectral attributes of optical images can reflect the metabolic rate and the heterogeneity of trees [44], [45], which may be able to replace DBH and improve the accuracy of volume estimation. Therefore, we assume that the fusion of optical and LiDAR multisource data based on the allometric growth model may be able to achieve large-scale and high-accuracy forest volume estimation.

In this article, we aim to propose a method of coupling allometric growth model and multisource data for forest volume estimation (CAMFVe), this is, the DBH in allometric growth model is replaced by the spectral index of optical images and the H is provided by canopy height obtained from LiDAR, realizing large-scale and high-accuracy forest volume estimation using remote sensing. To evaluate the CAMFVe method, we obtained ALS and TLS data covering four forest growth environments in Chengde City, then calculated and extracted forest volume and canopy height data. Combining canopy height data of LiDAR and the spectral index of optical images, the forest volume estimation model based on an allometric growth relationship was constructed. Finally, to evaluate the accuracy and applicability, the model by the CAMFVe method was compared with MLR, RF, and SVM models. We believe that the proposed method can realize large-scale and high-accuracy forest volume estimation, especially through the fusion of spaceborne LiDAR data and optical satellite images.

II. Materials

A. Study Area

The study area is located in Chengde City, Hebei Province, China (40°12′-42°37′N, 115°54′-119°15′E), with a temperate continental monsoon climate. The annual average temperature is 9.0 °C, the average annual precipitation is 402.3–882.6 mm, and the terrain is dominated by middle and low mountains and hills. Covering an area of 3.95 × 106 ha, Chengde was selected as a National Forest City in 2017, with rich forest resources and a forest coverage rate of 48%. The dominant tree species are *Larix principis-rupprechtii*, *Picea asperata*, and *Betula platyphylla*.

First, according to different canopy closures and terrain slopes, the forest of Chengde City was roughly classified into four types of forest growth environments using satellite images. According to the preliminary classification results, seven sites are selected in Chengde City [see Fig. 1(a)], with *Larix principis-rupprechtii* [see Fig. 1(c)] as the main tree species. Each site covers an area of 5–9 ha, with a total of 45.36 ha. The location, tree height, tree density, canopy closure, and terrain slope of each site varies, ensuring the representativeness of the proposed method. Two canopy closure categories (moderate and dense canopy closure having a canopy closure gradient of 0.4–0.6 and 0.6–0.8, respectively) [46], [47] and three slope

TABLE I
SUMMARY OF VEGETATION AND TERRAIN CONDITIONS OF THE SEVEN SITES

Study site	Number of plots	Area (ha)	Tree height (m)	Tree density (trees/ha)	Canopy closure	Slope (°)	Canopy closure class	Slope class
Site1	61	5.49	14.933	161.749	0.512	12.907	moderate	gentle
Site2	70	6.30	11.116	620.216	0.543	12.807	moderate	gentle
Site3	59	5.31	8.942	487.374	0.457	16.883	moderate	moderate
Site4	64	5.76	10.951	673.920	0.641	3.855	dense	flat
Site5	83	7.47	11.545	697.724	0.738	3.622	dense	flat
Site6	94	8.46	17.755	161.988	0.513	10.270	moderate	gentle
Site7	73	6.57	13.918	136.182	0.568	3.073	moderate	flat
All sites	504	45.36	13.017	419.879				

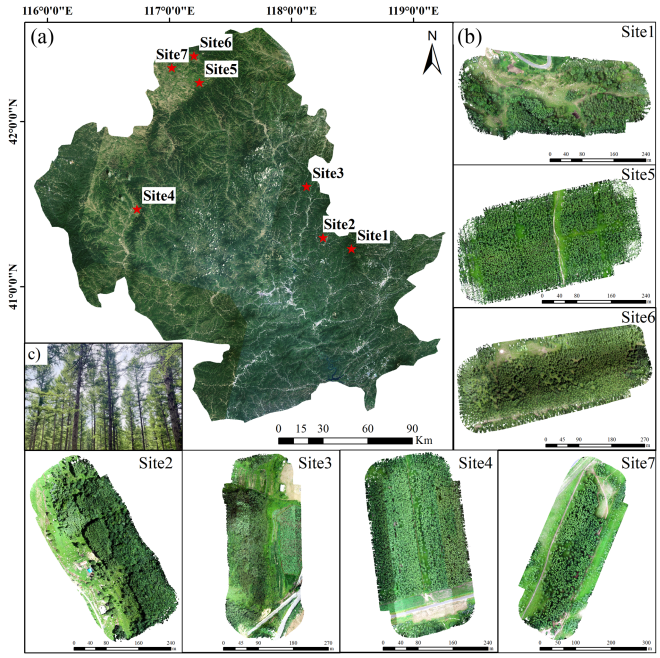

Fig. 1. Study area. (a) Geographic location of the study area. (b)ALS of seven sites displayed in RGB. (c) *Larix principis-rupprechtii*.

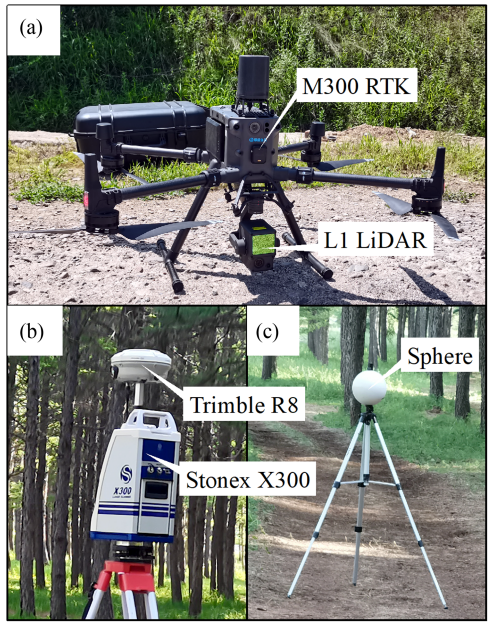

Fig. 2. Data acquisition. (a) DJI M300 RTK multirotor UAV and L1 sensor. (b) Trimble R8 and stonex X300. (c) Sphere.

gradient categories (flat, gentle, and moderate slope having a slope gradient of 0°–5°, 5°–15°, and 15°–30°, respectively) are identified [46], [48]. According to canopy closure and slope class, the study area is divided into four forest growth environments [see Fig. 1(b)], namely moderate canopy closure and flat slope (site7), moderate canopy closure and gentle slope (site1, site2, and site6), moderate canopy closure and moderate slope (site3), and dense canopy closure and flat slope (site4 and site5). The vegetation and terrain conditions of the seven sites are shown in Table I, where a plot corresponds to a Landsat pixel with a size of 30 m × 30 m. The number of plots is computed by the number of the Landsat pixel contained in each site. The area is the sum area of the plots in each site. The tree height is the average height of all individual trees in each site, and the individual tree height is calculated using the difference between the highest Z values recorded from the point cloud data and the digital elevation model (DEM) height. The tree density is the ratio of the number of trees obtained by individual tree segmentation to the area of the site. The canopy closure is the ratio of the number of vegetation canopy point clouds in the site to the total number of point clouds in the site, ranging from 0 to 1. The slope is calculated according to the DEM, which is converted from the extracted ground points.

B. ALS Data Acquisition and Processing

ALS data were acquired using DJI M300 multirotor UAV equipped with L1 sensor [see Fig. 2(a)] in July 2022, seven sites were acquired in total. The ALS system is equipped with a built-in RTK module, with a horizontal positioning accuracy of 10 mm + 1 ppm and a vertical positioning accuracy of 15 mm + 1 ppm. The L1 is capable of achieving high-precision positioning, with a ranging accuracy of 3 cm@100 m. The specification of the LiDAR is summarized in Table II. The UAV flight height is 80 m, the flight speed is 3.5 m/s, the side overlap rate is 80%, and the average point cloud density is 1851.14 pts/m^2.

ALS data were processed by ground point detection, point cloud normalization and high vegetation detection, individual tree trunk segmentation, and feature parameter extraction. First,

TABLE II
SPECIFICATIONS OF LASER SCANNING SYSTEMS

Technical specifications	ALS	TLS
Maximum distance range	450 m	300 m
Range systematic error	3 cm@100 m	4 mm@50 m
DGNSS precision	H: 10 mm+1 ppm V: 15 mm+1 ppm	H: 8 mm+0.5 ppm V: 15 mm+0.5 ppm
Laser wavelength	905 nm	905 nm
Scanning field of view	320°	360°*180°
Scanning speed	480 000 pts/s	40 000 pts/s
Angular accuracy	0.08°	0.37 mrad

TABLE III
PARAMETER SETTINGS IN TLS AND ALS DATA PROCESSING

Processing	Parameters	TLS	ALS
Ground point detection	Terrain inclination	60°	60°
	Iterative angle	6°	6°
	Iterative distance	0.2 m	0.6 m
Generation of CHM and high vegetation detection	Lower height value	0.2 m	2 m
	Higher height value	50 m	80 m
Individual tree trunk segmentation and feature parameter extraction	Average step length of trunk/canopy	0.15 m	2 m
	Growth step	0.5 m	1 m
	Minimum number of points contained in a single object	40	20

the points were separated into clusters using the segmentation algorithm based on smooth surface growth. The point cloud was filtered and the ground point was identified by the progressive densification filtering method of irregular triangular network, and the normalized digital surface model (CHM) was generated. Based on the normalized height of CHM, high vegetation was detected. Then, the individual tree parameters were extracted by point cloud segmentation method. The specific parameter settings of point cloud processing are shown in Table III. The results of individual tree segmentation based on ALS are shown in Fig. 3, where each of the four forest growth environments shows a 50 m × 50 m typical plot. As can be seen from Fig. 3, the ALS-based individual tree segmentation works well, and almost all individual trees are extracted accurately. Finally, the location of each extracted trunk ($\mathrm{Loc_{ALS}}$) is combined with the tree height (H_{ALS}), the crown diameter ($\mathrm{CD_{ALS}}$), and the diameter at breast height ($\mathrm{DBH_{ALS}}$) of ALS to form the ALS features dataset, which contains 23 245 trees. All the above processes are implemented in point cloud automata (PCA) v4.2.9.

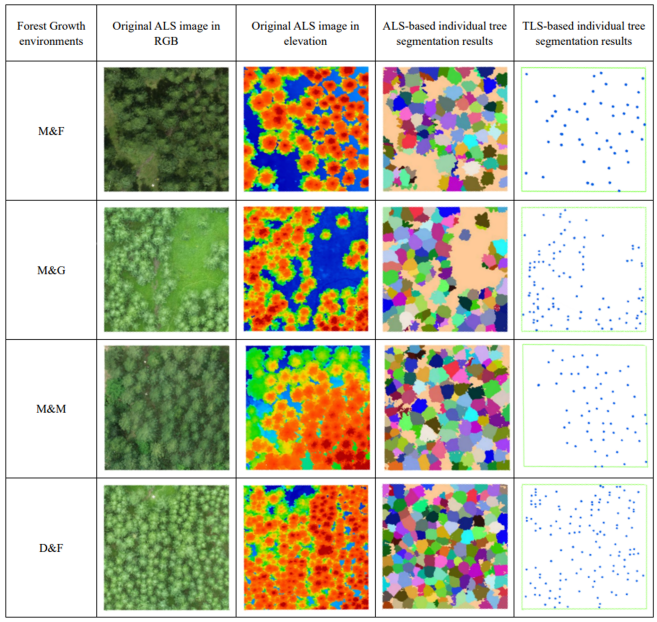

Fig. 3. Individual tree segmentation results of ALS and TLS. Note that M&F, M&G, M&M, and D&F represent the moderate canopy closure and flat slope, moderate canopy closure and gentle slope, moderate canopy closure and moderate slope, and dense canopy closure and flat slope, respectively. ALS-based individual tree segmentation results show the crown distribution of individual trees after segmentation basing ALS, and TLS-based individual tree segmentation results show the trunk distribution of individual trees after segmentation basing TLS.

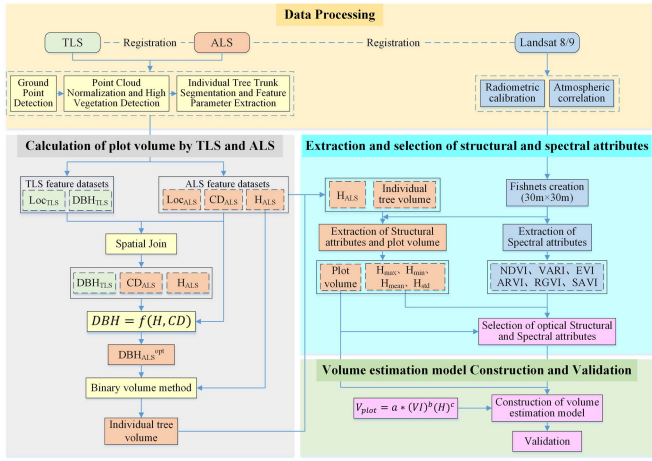

Fig. 4. Flowchart for forest volume estimation using CAMFVe.

C. TLS Data Acquisition and Processing

At the same time of ALS acquisition, TLS data were obtained using the Stonex X300 laser scanner [see Fig. 2(b)]. A total of seven blocks of TLS data were fetched, one for each site. Stonex X300 is a pulsed three-dimensional (3-D) laser scanner for precise measurement and rapid acquisition of massive 3-D point cloud data in complex environments. The accuracy and distance of measurement are ±4 mm@50 m and 300 m, respectively. The data were obtained in a fine mode with an average point cloud density of 2928.98 pts/m^2.

TABLE IV
DESCRIPTION OF THE COLLECTED LANDSAT IMAGES

Study Site	Date acquired	Image name	Row–column number
Site1, Site2, Site3	2022.08.10	Landsat 9	122 031
Site4, Site5, Site6, Site7	2022.07.24	Landsat 8	123 031

Trimble R8 [see Fig. 2(b)] was used to measure the geographic coordinates of the TLS base station and sphere [see Fig. 2(c)], and the single station orientation method [49] was employed to the TLS data for registration with ALS. The point cloud processing of TLS is similar to ALS but with different parameters. The specific parameter settings are shown in Table III. The results of individual tree segmentation based on TLS are shown in Fig. 3, where each of the four forest growth environments shows a 50 m × 50 m typical plot. As can be seen from Fig. 3, the TLS-based individual tree segmentation works well, and almost all individual trees are extracted accurately. Finally, the location of each extracted trunk ($\mathrm{Loc_{TLS}}$) is combined with the diameter at breast height of TLS ($\mathrm{DBH_{TLS}}$) to form the TLS features dataset, which contains a total of 1741 trees. All the above processes are implemented in PCA v4.2.9.

D. Landsat Data Acquisition and Processing

For each study site, we downloaded the Landsat 8/9 Collection2 level1 Tier1 images from July to August 2022 with less than 5% cloud cover from USGS.[1] Two Landsat images were selected, which covered the study area and met the time and space requirements for conducting research. The specific information of images is shown in Table IV. Then, the images were processed by radiometric calibration, atmospheric correction, mosaic, clipping, etc. Finally, the Landsat images and the acquired ALS data were georegistered using the artificial ground objects in the images as the control points, which allows for a reasonably accurate matching between the trees of ALS data and the pixels of Landsat images.

III. METHODS

A. Coupling Allometric Growth Model and Multisource Data for Forest Volume Estimation

In this article, we proposed a method of coupling vegetation index (VI) with allometric growth model for forest volume estimation. The specific form of the proposed method is given as follows:

$$V_{\mathrm{plot}} = a*(\mathrm{VI})^b(H)^c \tag{1}$$

where V_{plot} is the forest volume of the plot, VI is the optimal VI on the plot scale, H is the optimal canopy height parameter on the plot scale, and a, b, and c are the model coefficients to be obtained.

[1][Online]. Available: https://earthexplorer.usgs.gov/

TABLE V
STRUCTURAL ATTRIBUTES AND SPECTRAL INDICES EXTRACTED FROM ALS AND LANDSAT

Parameters	Abbreviation	Description	Reference
Structural attributes	H_{max}	Maximum canopy height in a plot	[51]
	H_{min}	Minimum canopy height in a plot	[51]
	H_{mean}	Mean canopy height in a plot	[51]
	H_{std}	The standard deviation of canopy height in a plot	[51]
Spectral indices	NDVI	Normalized Difference Vegetation Index, $NDVI = (NIR - R)/(NIR + R)$	[52]
	VARI	Visible Atmospheric Resistant Index, $VARI = (G - R)/(G + R - B)$	[53]
	EVI	Enhanced Vegetation Index, $EVI = [2.5(NIR - R)]/(NIR + 6R - 7.5B + 1)$	[54]
	ARVI	Atmospherically Resistant Vegetation Index, $ARVI = (NIR - (2R) + B)/(NIR + (2R) + B)$	[55]
	RGVI	Red–Green Vegetation Index, $RGVI = (R - G)/(R + G)$	[55]
	SAVI	Soil-Adjusted Vegetation Index, $SAVI = (1 + 0.5)(NIR - R)/(NIR + R + 0.5)$	[56]

Note: R, G, B, and NIR represent the red, green, blue, and near-infrared bands of Landsat images, respectively.

We explored the feasibility of CAMFVe method mainly from the following steps (Fig. 4). The first step is to construct the DBH ($\mathrm{DBH^{opt}_{ALS}}$) estimation model of ALS to obtain the $\mathrm{DBH^{opt}_{ALS}}$ of the study area by using the diameter at breast height of TLS ($\mathrm{DBH_{TLS}}$) as a reference. Then, $\mathrm{DBH^{opt}_{ALS}}$ and tree height of ALS (H_{ALS}) are input into the allometric growth model (binary volume equation). Thus, more accurate individual tree volume and plot volume in the study area are obtained. The second step is to use the upscaling aggregation method to extract the spectral and structural attributes (Table V) on the 30-m plot scale, and the best spectral and structural attributes for forest volume estimation are selected. The third is to build a forest volume estimation model coupling VI with an allometric growth model and apply it to the study area.

1) Calculation of Plot Volume by TLS and ALS: Calculation of plot volume by TLS and ALS is the first step of CAMFVe method, which includes three steps. First, the feature-level fusion of TLS and ALS is realized by spatial join [28]. Second, using $\mathrm{DBH_{TLS}}$ as the reference, the DBH estimation model is constructed. Third, the model is applied to the entire ALS region, and $\mathrm{DBH^{opt}_{ALS}}$ and H_{ALS} are the inputs into the allometric growth model to obtain accurate individual tree volume and plot volume in the study area.

a) Feature-level fusion through spatial join: The trunk locations ($\mathrm{Loc_{TLS}}$ and $\mathrm{Loc_{ALS}}$) of georeferenced TLS and ALS are very close, and the feature-level fusion of the two can be achieved through spatial join. In this study, the maximum search radius of spatial join is set as 2 m according to the tree trunk location distribution of the two datasets. As a result, 1741 groups of H_{ALS}, $\mathrm{CD_{ALS}}$, and $\mathrm{DBH_{TLS}}$ were obtained, i.e., 1741 trees were tallied.

b) Construction of DBH estimation model: Since the laser cannot directly penetrate the forest canopy when the stand is

dense, DBH_{ALS} obtained by ALS is not accurate enough, so the DBH of ALS is usually estimated using tree height and canopy diameter. In this article, an MLR model for DBH_{ALS}^{opt} estimation is constructed using DBH_{TLS} as a reference and CD_{ALS} and H_{ALS} as dependent variables. R^2 and RMSE are used as indicators to evaluate the accuracy of the model. Total 70% of the data are used for training and 30% for verification.

c) Calculation of individual tree and plot volume: The constructed DBH estimation model is applied to ALS to obtain more accurate DBH_{ALS}^{opt}. DBH_{ALS}^{opt} and H_{ALS} are input into the allometric growth model [50] of *Larix principiss-rupprechtii*, and the accurate individual tree volume is obtained

$$V_{tree} = 0.00005741 * D^{1.77035219} * H^{1.12503045} \quad (2)$$

where D is the stem diameter at breast height in cm, H is the tree height in m, and V_{tree} is the individual tree volume in m^3.

The study area is divided into 30 m × 30 m sampling plots according to Landsat pixels, with a total of 504 plots. Given that the volume of trees is primarily contributed by the trunk, the center position of the trunk is used as the actual position of individual trees for matching to the pixels of Landsat images. Individual tree volumes are upscaled and aggregated onto 30-m plots using the zonal statistic tool in the ArcGIS Pro software (Esri, Inc.). Finally, the volume of each plot is calculated as the ratio of the total volume of all individual trees in the plot to the area of the plot and is used as the ground truth (field measurement data) in the following model construction and verification.

2) Extraction and Selection of Structural and Spectral Attributes: Four structural attributes and six spectral indices (Table V) are extracted and upscaled onto 30-m plots from ALS and Landsat using the zonal statistic tool in the ArcGIS Pro software (Esri, Inc.).

The canopy height-related parameters H_{max}, H_{min}, H_{mean}, and H_{std} are the maximum, minimum, average, and standard deviation of all individual tree heights in each 30 m × 30 m plot. These attributes can represent the vertical distribution of the canopy (H_{max}, H_{min}, H_{mean}) and explain the complexity and heterogeneity of the vertical structure of the canopy (H_{std}) [38]. Structural parameters, such as NDVI and EVI, are sensitive to forest volume and biomass, which can effectively measure vegetation growth and are widely used in volume estimation [52], [53], [54], [55], [56].

Owing to the heterogeneity of forest stands, the optimal structural and spectral parameters differ across study sites. Simple regression models are implemented to test the ability of each variable to predict volume in the seven study sites with R^2 as an evaluation indicator. In order to construct a general and robust model suitable for different forest growth environments and stand characteristics, the cumulative *R*-squared [51] is used to select the optimal structural and spectral parameters. The parameter with the highest cumulative R^2 in different study sites is selected as the optimal parameter, which is used for the construction and verification of subsequent forest volume models.

3) Construction of Volume Estimation Model: With the plot volume as the dependent variable and the optimal structural and spectral parameters as the independent variable, Levenberg–Marquardt [57] is used as the global optimization algorithm to find the most suitable model parameter values for (1). The stratified random sampling method is used to sample the plot volumes, the optimal structural, and spectral parameters data. Total 70% of the plots are randomly selected for training to construct a volume estimation model, and 30% are verified for model accuracy.

B. Validation

To evaluate the performance of the proposed CAMFVe method, the accuracy is evaluated from two aspects: DBH estimation model accuracy and volume estimation model accuracy.

For the accuracy of the DBH estimation model, DBH_{ALS}^{opt} estimated by the DBH estimation model, constructed by TLS and ALS, is compared with DBH_{ALS} directly extracted by ALS, using DBH_{TLS} as a reference. R^2, RMSE, mean, maximum (max), minimum (min), standard deviation (std), and mean absolute error (ME) of DBH_{ALS}^{opt} and DBH_{ALS} are calculated and statistically analyzed

$$R^2 = 1 - \frac{\sum_{i=1}^{n} (y_i - \widehat{y}_i)^2}{\sum_{i=1}^{n} (y_i - \bar{y})^2} \quad (3)$$

$$\text{RMSE} = \sqrt{\frac{\sum_{i=1}^{n} (y_i - \widehat{y}_i)^2}{n}} \quad (4)$$

$$\text{RRMSE} = \frac{\text{RMSE}}{\bar{y}} \times 100\% \quad (5)$$

$$\text{ME} = \frac{1}{n} \sum_{i=1}^{n} | y_i - \bar{x} | \quad (6)$$

where n is the number of testing plots; y_i and $\widehat{y}_i$ represent the measured and predicted volume in plot i, respectively; and $\bar{y}$ is the mean of measured volume.

For the accuracy of volume estimation model, with the measured volume as reference and R^2, RMSE, and RRMSE as evaluation indicators, the estimation accuracy of volume estimation model in all sites and four forest growth environments is evaluated using 30% validation plots. GEDI and Landsat 8/9 data are used to apply the model to the entire Chengde city. And the accuracy evaluation of the volume estimation results in Chengde City is conducted using the data of the overlapping part of the GEDI footprints data in 30% of verification plots. Finally, to evaluate the accuracy of the proposed CAMFVe method, the volume estimation accuracy of CAMFVe is further compared with the commonly used machine learning regression methods, including MLR, RF, and SVM. In keeping with the proposed method, the three machine learning regression models are also trained and validated using the same plot data.

IV. Results

A. Results Accuracy of DBH Estimation Model

Three DBHs obtained in different ways are shown in Fig. 5. The *X*-axis is the tree ID, and the *y*-axis represents the DBH value. DBH_{TLS} (black), extracted from TLS, is used as a reference due to the high accuracy, and the Tree IDs are arranged in ascending order according to the DBH_{TLS} value. DBH_{ALS} (red) is obtained directly from ALS, and DBH_{ALS}^{opt} (blue) is calculated

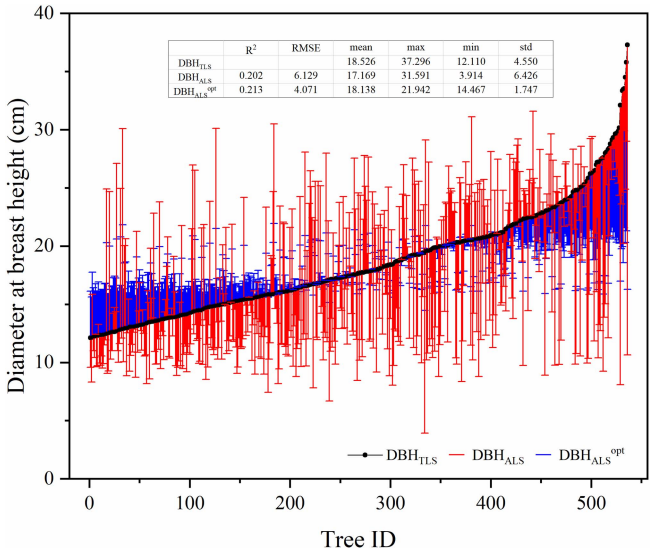

	R^2	RMSE	mean	max	min	std
DBH_{TLS}			18.526	37.296	12.110	4.550
DBH_{ALS}	0.202	6.129	17.169	31.591	3.914	6.426
DBH_{ALS}^{opt}	0.213	4.071	18.138	21.942	14.467	1.747

Fig. 5. DBH of 536 trees extracted by TLS and ALS.

using the DBH estimation model of (7). The corresponding statistics of R^2, RMSE, mean, std, and so on of the three DBHs are shown in Fig. 5

$$\mathrm{DBH}_{\mathrm{ALS}}^{\mathrm{opt}} = 0.3132 * H_{\mathrm{ALS}} + 0.3751 * \mathrm{CD}_{\mathrm{ALS}} + 11.26. \quad (7)$$

It can be seen from the reference ($\mathrm{DBH}_{\mathrm{TLS}}$) that the DBH of trees in the study area varies greatly from 12.11 to 37.296 cm. Both $\mathrm{DBH}_{\mathrm{ALS}}$ and $\mathrm{DBH}_{\mathrm{ALS}}^{\mathrm{opt}}$ have certain deviations and the deviations have certain rules. When $\mathrm{DBH}_{\mathrm{TLS}}$ is between 12.11 and 26.343 cm, $\mathrm{DBH}_{\mathrm{ALS}}$ is seriously overestimated and underestimated. When the $\mathrm{DBH}_{\mathrm{TLS}}$ is between 26.343 and 37.296 cm, $\mathrm{DBH}_{\mathrm{ALS}}$ is seriously underestimated. When $\mathrm{DBH}_{\mathrm{TLS}}$ ranges from 12.11 to 16.274 cm, $\mathrm{DBH}_{\mathrm{ALS}}^{\mathrm{opt}}$ is slightly overestimated. When $\mathrm{DBH}_{\mathrm{TLS}}$ is between 16.274 and 19.621 cm,$\mathrm{DBH}_{\mathrm{ALS}}^{\mathrm{opt}}$ has the best estimation effect. When $\mathrm{DBH}_{\mathrm{TLS}}$ range from 19.621 to 37.296 cm, $\mathrm{DBH}_{\mathrm{ALS}}^{\mathrm{opt}}$ is slightly underestimated. The estimation accuracy of $\mathrm{DBH}_{\mathrm{ALS}}^{\mathrm{opt}}$ (RMSE = 4.071 cm and ME = 0.388 cm) is much higher than that of $\mathrm{DBH}_{\mathrm{ALS}}$ (RMSE = 6.129 cm and ME = 1.357 cm). Compared with $\mathrm{DBH}_{\mathrm{ALS}}$, $\mathrm{DBH}_{\mathrm{ALS}}^{\mathrm{opt}}$ has a better estimation effect, with a 33.578% reduction in RMSE and 71.408% in ME.

B. Selection of Structural and Spectral Attributes

The R^2 values from simple regression models based on different parameters in all study sites are shown in Fig. 6.

For structural attributes, H_{mean} performs best across all sites in estimating volume, with the highest cumulative R^2 (4.154). H_{mean} performs best on all sites except site1 (moderate canopy closure and gentle slope). The estimation accuracy of $H_{\max}$, $H_{\min}$, and H_{std} varies in different sites. H_{mean}, $H_{\max}$, and $H_{\min}$ are the parameters that characterize the vertical distribution of canopy height. H_{mean} and $H_{\max}$ perform best in site3 (moderate canopy closure and moderate slope), and $H_{\min}$ performs best in site7 (moderate canopy closure and flat slope). H_{std}, which represents vertical structural complexity and heterogeneity of

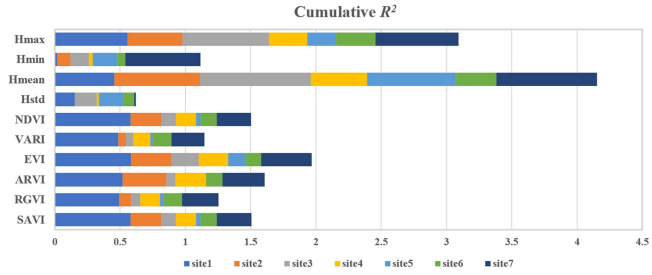

Fig. 6. Stacked bar plots of the R^2 values from simple regression models based on different parameters in all study sites.

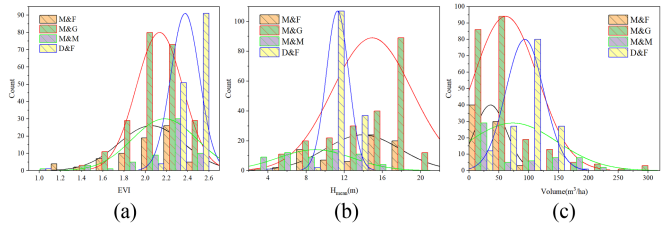

Fig. 7. Data distribution of (a) spectral parameter (EVI), (b) structural parameter (H_{mean}), and (c) plot volume in different forest growth environments.

canopy distribution, performs best in site5 (dense canopy closure and flat slope).

For spectral attributes, EVI performs best across all sites in estimating volume, with the highest cumulative R^2 (1.966). EVI performs best on all sites except site2 and site6 (moderate canopy closure and gentle slope). All parameters perform best in site1 (moderate canopy closure and gentle slope). Except EVI, R^2 of all other parameters are lowest in site5 (dense canopy closure and flat slope). EVI is not only suitable for sparse vegetation but also suitable for dense vegetation compared with other VIs, which is because EVI reduces the influence of "saturation effect."

Since H_{mean} and EVI show the best overall performance across all sites, they are used to construct models in CAMFVe. Furthermore, the EVI, H_{mean}, and plot volume distribution histograms of four different forest growth environments are shown in Fig. 7.

The EVI, H_{mean}, and volume of the four forest growth environments present a normal distribution, and there is a substantial gradient among different forest growth environments. The distribution of EVI (0.940–2.511), H_{mean} (2.915–20.380 m), and plot volume (0.308–312.372 m^3/ha) demonstrates that the sites we selected could well represent forests in different growth environments.

C. Performance of the Proposed Method

The volume estimation models for all plots and four different forest growth environments are shown in Table VI, and the scatter plots of measured and predicted volume of all plots and different forest growth environments by the CAMFVe method are shown in Fig. 8.

It can be found that our proposed method has achieved good prediction accuracy in all plots and different forest growth environments, and models based on specific forest growth environments are more accurate than the model of all plots. The

TABLE VI
SUMMARY OF VOLUME ESTIMATION MODELS FOR FOUR FOREST GROWTH ENVIRONMENTS

Forest growth environments	Model	Mean Volume	Std Volume
All plots	$V = 0.012 * EVI^{8.158} * H_{mean}{}^{0.888}$	68.553	51.769
Moderate canopy closure and Flat slope	$V = 0.003 * EVI^{1.249} * H_{mean}{}^{3.097}$	30.070	26.574
Moderate canopy closure and Gentle slope	$V = 0.002 * EVI^{8.986} * H_{mean}{}^{1..220}$	61.511	53.622
Moderate canopy closure and Moderate slope	$V = 0.003 * EVI^{6.131} * H_{mean}{}^{2.315}$	73.364	73.939
Dense canopy closure and Flat slope	$V = 0.010 * EVI^{3.331} * H_{mean}{}^{2.644}$	93.531	31.776

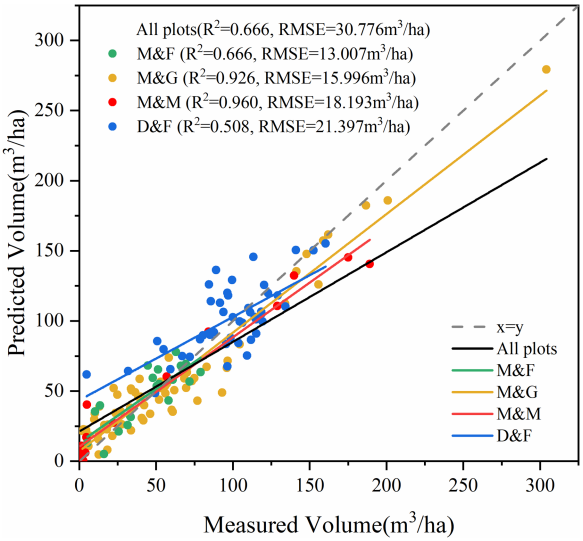

Fig. 8. Measured and predicted volume from CAMFVe for all plots and different forest growth environments.

CAMFVe method achieved the highest R^2 in moderate canopy closure and moderate slope, the lowest RMSE in moderate canopy closure and flat slope, and the lowest R^2 and the highest RMSE in dense canopy closure and flat slope. The canopy closure class (Moderate) remains unchanged, the steeper the slope, the higher the R^2, but the higher the RMSE, and the lower the estimation accuracy. With slope class (Flat) unchanged, the lower the canopy closure, the higher the R^2, the lower the RMSE, and the higher the estimation accuracy. At moderate canopy closure sites, the predicted and measured volumes are all around the 1:1 line. At dense canopy closure sites, the proposed method also does not produce large overestimates and underestimates in areas with low and high volumes.

Fig. 9 shows the volume of the study area estimated by the CAMFVe method for each site and the GEDI transit area of Chengde City, with a spatial resolution of 30 m. Fig. 10 shows the scatter plot between the measured volume and the volume estimated by GEDI and Landsat.

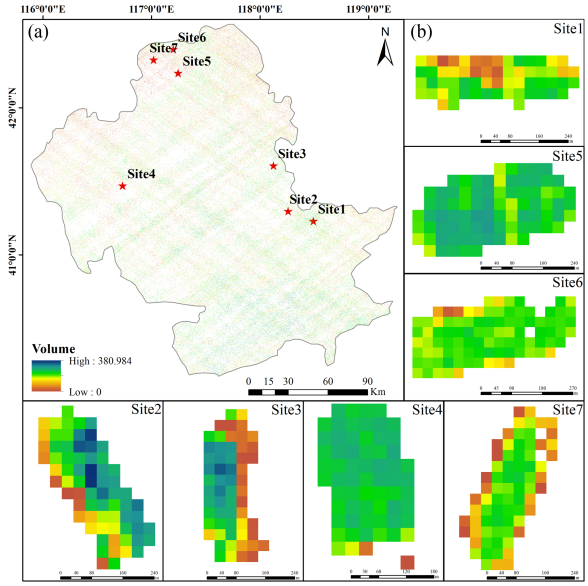

Fig. 9. Volumes of the study area estimated by CAMFVe. (a) Volume of Chengde city estimated by rh98 of GEDI and EVI of Landsat. (b) Volume of site1–7 estimated by H_{mean} of ALS and EVI of Landsat.

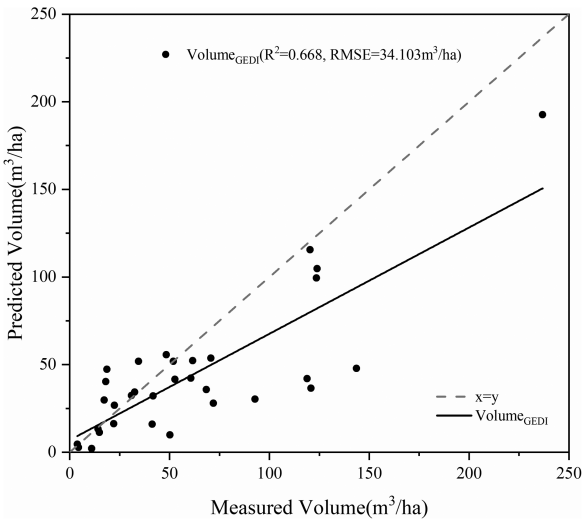

Fig. 10. Scatter plot between the measured volume and predicted volume$_{\text{GEDI}}$.

It can be seen that our method is suitable for different sites and is sensitive to both high and low volume. Compared with the measured volume, the R^2 and RMSE of the predicted volume, estimated by the canopy height of GEDI and spectral attribute of Landsat, are 0.668 and 34.103 m^3/ha, respectively. Therefore, the proposed CAMFVe method can realize large-scale and high-accuracy forest volume estimation, especially through the fusion of spaceborne LiDAR data and optical satellite images.

D. Comparison With Existing Methods

Fig. 11 and Table VII present scatter plots and validation statistics for volume estimation using different model scenarios for different forest growth environments, respectively.

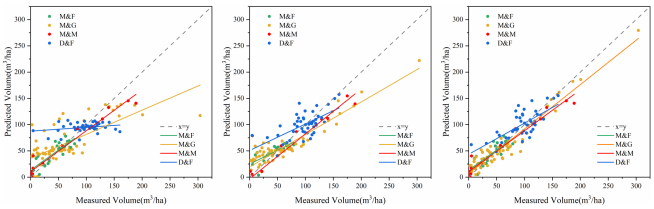

Fig. 11. Comparisons between measured volume and predicted volume by using different model scenarios for different forest growth environments. (a) Predicted volume is estimated only by EVI data. (b) Predicted volume is estimated only by H_{mean} data. (c) Predicted volume is estimated by combining EVI with H_{mean} using the CAMFVe method.

In combination with Fig. 11 and Table VII, it can be found that, compared with the methods using only structural or spectral information, the forest volume obtained by CAMFVe has higher R^2 and lower RMSE. For different forest growth environments, the addition of spectral parameter EVI improves the estimation ability compared with H_{mean}-based model, especially moderate canopy closure and moderate slope, with R^2 increasing by 0.116 and RMSE decreasing by 20.170%. For all data, our method has a better estimation accuracy (a reduction of 28.502% in RMSE) than the H_{mean}-based model. The estimation ability of the model using only spectral attributes is poor, and the scatter plot between the measured and predicted volume is very scattered. The distribution of points after the fusion of structural attributes using the CAMFVe method is more compact, and the estimation accuracy is greatly improved (see Fig. 11). In general, using the spectral information as an auxiliary, the RMSE of volume estimation can be reduced by 10.152% (see Table VII).

It can be seen from Table VII that compared with MLR, RF, and SVM methods, CAMFVe has better volume estimation ability. For all plots, CAMFVe has the highest accuracy compared with all other methods except MLR_All parameters (R^2 higher 0.011 and RMSE lower 0.847% than CAMFVe) and RF_All parameters (R^2 higher 0.047 and RMSE lower 3.663% than CAMFVe). For different forest growth environments, except MLR_All parameters for moderate canopy closure and gentle slope, and dense canopy closure and flat slope, the R^2 is 0.004 and 0.128 higher than CAMFVe, and the RMSE is 1.838% and 3.633% lower than CAMFVe, respectively. For all other forest growth environments and all methods, CAMFVe method has the highest accuracy. It can be seen that our method can improve the estimation accuracy in most forest growth environments. In addition, the CAMFVe method only uses two parameters as predictive variables. Compared with MLR, RF, SVM, and other machine learning methods, CAMFVE method requires fewer parameters, has higher accuracy, and is simpler and more efficient.

TABLE VII
VALIDATION STATISTICS FOR VOLUME ESTIMATION USING DIFFERENT MODEL SCENARIOS FOR DIFFERENT FOREST GROWTH ENVIRONMENTS

Forest growth environment	Methods	Independent Variable	R^2	RMSE	RRMSE
All plots	CAMFVe	H_{mean}, EVI	0.666	30.776	43.588
	VI_based	EVI	0.350	42.739	60.532
	H_based	H_{mean}	0.071	50.899	72.090
	MLR	H_{mean}, EVI	0.444	39.935	56.562
	MLR	All parameters	0.677	30.177	42.741
	RF	H_{mean}, EVI	0.651	31.268	44.286
	RF	All parameters	0.713	28.189	39.925
	SVM	H_{mean}, EVI	0.446	49.597	70.245
	SVM	All parameters	0.443	44.774	63.415
Moderate canopy closure and flat slope	CAMFVe	H_{mean}, EVI	0.666	13.007	29.416
	VI_based	EVI	0.355	18.358	41.517
	H_based	H_{mean}	0.611	14.139	31.977
	MLR	H_{mean}, EVI	0.594	14.365	32.487
	MLR	All parameters	0.596	14.451	32.681
	RF	H_{mean}, EVI	0.615	13.991	31.642
	RF	All parameters	0.652	13.377	30.254
	SVM	H_{mean}, EVI	0.599	21.173	47.884
	SVM	All parameters	0.486	16.643	37.640
Moderate canopy closure and gentle slope	CAMFVe	H_{mean}, EVI	0.926	15.996	26.356
	VI_based	EVI	0.518	38.874	64.049
	H_based	H_{mean}	0.860	25.582	42.150
	MLR	H_{mean}, EVI	0.900	19.089	31.452
	MLR	All parameters	0.930	14.883	24.521
	RF	H_{mean}, EVI	0.871	20.502	33.779
	RF	All parameters	0.741	28.284	46.601
	SVM	H_{mean}, EVI	0.371	47.090	77.586
	SVM	All parameters	0.428	44.175	72.784
Moderate canopy closure and moderate slope	CAMFVe	H_{mean}, EVI	0.960	18.193	35.510
	VI_based	EVI	0.160	71.517	139.590
	H_based	H_{mean}	0.844	28.527	55.680
	MLR	H_{mean}, EVI	0.847	27.335	53.354
	MLR	All parameters	0.873	26.478	51.681
	RF	H_{mean}, EVI	0.888	28.905	56.418
	RF	All parameters	0.881	24.161	47.158
	SVM	H_{mean}, EVI	0.816	63.887	124.698
	SVM	All parameters	0.576	57.713	112.646
Dense canopy closure and flat slope	CAMFVe	H_{mean}, EVI	0.508	21.397	21.974
	VI_based	EVI	0.065	28.738	29.514
	H_based	H_{mean}	0.403	23.472	24.105
	MLR	H_{mean}, EVI	0.452	22.328	22.930
	MLR	All parameters	0.636	17.859	18.341
	RF	H_{mean}, EVI	0.457	22.400	23.004
	RF	All parameters	0.372	24.154	24.806
	SVM	H_{mean}, EVI	0.004	29.920	30.727
	SVM	All parameters	0.037	29.054	29.838

V. DISCUSSION

There are two challenges in large-scale and high-accuracy forest volume estimation: First, obtaining large-scale forest structural and spectral information simultaneously; second, whether sufficient measurement data can be obtained [24], [42], [58]. To address these limitations, based on the allometric model, we coupled VI and structural attributes at the satellite pixel scale to achieve large-scale and high-accuracy forest volume estimation.

A. Calculation of Plot Volume by TLS and ALS

Traditionally, the forest volume is usually calculated by inputting the tree height and DBH into the allometric growth model, but the tree height and DBH are difficult to obtain in a large range. The traditional manual measurement method is time-consuming and laborious. The wide application of UAV

LiDAR makes it possible to obtain forest structural attributes, such as tree height and DBH quickly and in a wide range. ALS can obtain H with high accuracy [27], but accurate DBH information cannot be obtained [28]. Guo et al. [28] directly extract DBH from ALS through software, and the accuracy is not high. There are also some studies that estimate the DBH through the H and/or CD, but the accuracy is still not satisfactory [59], [60]. TLS has been proven to be an effective way to obtain high-accuracy DBH with an error not exceeding 1 cm [29], [30], but the accuracy of H needs to be improved. There are studies on high-precision fusion of TLS and ALS to obtain accurate DBH and H [61], [62], which is highly accurate but difficult to be applied in a wide range due to complex processing. In this article, feature-level fusion of TLS and ALS is performed using spatial join, and DBH estimation model of ALS is constructed based on $\mathrm{DBH_{TLS}}$. Finally, we use $\mathrm{DBH_{TLS}}$ as a reference, which is currently the most effective means of obtaining high-accuracy DBH on a large scale to verify the accuracy of the DBH estimation model. With $\mathrm{DBH_{TLS}}$ as the reference, the RMSE and ME of $\mathrm{DBH_{ALS}^{opt}}$ are 4.071 cm and 0.388 cm, respectively. Compared with $\mathrm{DBH_{ALS}}$ extracted directly from ALS, $\mathrm{DBH_{ALS}^{opt}}$ reduced RMSE by 33.578% and ME by 71.408%. This is consistent with the result of Guo et al. [28]. By using the spatial join and feature-level fusion method of ALS and TLS, we do not need a large number of measured DBH as training data, but only need to perform simple feature-level fusion of TLS and ALS, which can achieve accurate DBH estimation based on the tree height and crown width of ALS so as to obtain accurate volume data in ALS region. With the continuous improvement of laser measurement and technology, the accuracy of TLS to obtain DBH will increase, and the accuracy of the DBH estimation model will also increase accordingly.

B. Large-Scale Volume Estimation by VI Instead of DBH

By coupling VI and allometric growth model, the CAMFVe method uses VI instead of DBH to estimate forest volume. In the process of model construction, the cumulative R^2 is used to select the optimal structural and spectral parameters. And we found that for different forest growth environments, H_{mean} is the best structural attribute for volume estimation, which is consistent with Yang et al.'s article [51]. No matter whether the stand is homogeneous or not, H_{mean} can reflect the forest structure and stand growth [63]. In addition, we found that EVI has the best performance in different forest growth environments, which is inconsistent with the best performance of NDVI [64]. The cumulative R^2 is susceptible to the influence of a particular sample point and does not necessarily indicate that EVI is superior to NDVI. Therefore, in order to verify the feasibility of the cumulative R^2 method, all plots were used to analyze the correlation between the six spectral parameters and forest volumes. And it was found that EVI was the optimal spectral parameter, which is consistent with the cumulative R^2 method. In further analysis, we found that this is because the canopy closure of our study area ranges from 0.457 to 0.738, and the grades are both moderate and dense. NDVI will be affected by "saturation effect" at high canopy closure, and the estimation accuracy will be reduced. EVI is an improvement relative to NDVI, which reduces the influence of vegetation "saturation effect" [64]. It is not only suitable for sparse vegetation but also suitable for dense vegetation compared with other VIs.

By fusing optimal structural and spectral attributes, our method achieves good results. For the generalized model constructed by all plots, the R^2 of our method reaches 0.666 and the RRMSE is 43.588%. For different forest growth environments, the accuracy is different, with R^2 ranging from 0.508 to 0.960 and RRMSE ranging from 21.974% to 35.510%. This is mainly caused by the different forest canopy closure and slope categories of different sites. EVI reflects the spectral characteristics of the forest canopy. When the canopy closure is high, EVI is also affected by "saturation effects" slightly, and the difference of saturation effect is different for different canopy closure categories. H reflects the average growth condition of trees in the plot, but the extraction accuracy of H is affected by the change of slope. It is difficult to obtain the accurate forest volume using structural or spectral attributes alone for forests with complex structures. Our method couples the structural and spectral attributes based on the allometric growth model, and the RRMSE is reduced by 28.502% compared with the H_{mean}-based model. This is mainly because the added spectral attribute provides information on the spectral heterogeneity of forest canopy, which can reflect the diversity of forest volume.

MLR, RF, and SVM are commonly used machine learning models for forest volume estimation [35], [37], [39]. Compared with these machine learning methods, our CAMFVe method has a higher volume estimation accuracy. This indicates that it is feasible to estimate the volume based on the allometric growth model coupling structural and spectral attributes. However, the results of RF and MLR using all variables for all plots are slightly better than our method (R^2 increased by 0.011 and 0.047, and RMSE decreased by 0.847% and 3.663%, respectively). This may be due to the combination of multiple variables, but this leads to the invisibility of the model and complexity of the method. In addition, these machine learning methods require many parameters as input data, which may cause collinearity problems [40] and may not necessarily improve the accuracy of volume estimation. Compared with these machine learning methods, our method is more convenient to fit and can provide explicit calculation formulae, which is more suitable for large-scale and rapid forest volume estimation.

C. Uncertainty and Outlook

The CAMFVe method is simple and robust, which provides a fast and high-accuracy method to obtain a large range of forest volume using remote sensing. Existing spaceborne LiDAR (GEDI and ICESat-2, etc.) provides nearly global coverage, uniform distribution, and high-density ground sampling footprints that can be used to obtain canopy height data. In addition, the existing optical remote sensing satellites, such as Landsat, Sentinel-2, and GF-2, can catch forest heterogeneity well. In the future, images with higher spatial and spectral resolution, different VIs, and spaceborne LiDAR can be combined for volume retrieval at regional and global scales.

However, there are still some limitations in this study. One of the shortcomings of our method is that the accurate registration of ALS and Landsat images is required; otherwise, the model accuracy will be affected. In this article, although we used artificial ground objects to perform accurate registration of ALS and Landsat images, due to the significant difference in spatial resolution between the two, the registration accuracy still needs to be improved. In the future, with the improvement of more and better registration methods, the accuracy of our model will be correspondingly higher. The study area of this article is Chengde City, Hebei Province. The main tree species in Chengde city is *Larix principis-rupprechtii*, and the predominant terrain consists of medium–low mountains and hills. Therefore, in our study area, the main tree species is *Larix principis-rupprechtii*, the slope categories include only flat, gentle, and moderate, and the canopy closure categories include only moderate and dense. The applicability of this method has not been verified for other tree species, canopy closure, and slope categories. More tree species, canopy closure, and slope categories can be explored in the future. In addition, since GEDI provides footprint data, this article only utilizes the combination of GEDI footprints and Landsat data in 2022 to apply the CAMFVe method to Chengde City. As a result, the volume results are not spatially continuous. In future research, GEDI, ICESat-2, and other data sources can be combined to generate spatially continuous canopy height data, which can then be integrated with spectral attributes from optical satellite images to obtain spatially continuous volume data.

VI. Conclusion

In this study, a forest volume estimation method based on an allometric growth model combining VI of optical images and canopy height of LiDAR is proposed. To explore the applicability of the method, the volume estimation model based on the allometric growth model, combining the canopy height of ALS and the VI of Landsat, is constructed with reference to the volume calculated jointly by ALS and TLS. The applicability of the model is evaluated under different forest canopy closure and slope categories, and the accuracy is compared with MLR, RF, and SVM methods. The results show that the DBH estimation model constructed by TLS and ALS can improve the DBH calculation accuracy of ALS with a 2.058 cm reduction in RMSE, which can realize the high-accuracy DBH calculation of ALS. The H_{mean} and EVI are the optimal structural and spectral attributes for different forest growth environments. The CAMFVe method is applicable to almost all forest growth environments. Compared with the H_{mean}-based model, the addition of spectral attribute improves the estimation accuracy of volume with a 10.152% reduction in RMSE. Furthermore, the CAMFVe method outperforms RF, SVM, and other machine learning methods, offering higher accuracy, requiring fewer parameters, and being simpler and more efficient. The proposed method, based on an allometric growth model and utilizing VI instead of DBH, enables large-scale and high-accuracy forest volume estimation, particularly through the fusion of spaceborne LiDAR data and optical satellite images. In the future, we can integrate more spaceborne LiDAR and optical satellite images to conduct larger scale, higher accuracy, and spatially continuous volume estimation studies.

Acknowledgment

We would like to thank Z. Lu and K. Wang for their valuable support.

References

[1] Y. Pan et al., "A large and persistent carbon sink in the world's forests," *Science*, vol. 333, pp. 988–993, 2011.
[2] E. Vangi et al., "Large-scale high-resolution yearly modeling of forest growing stock volume and above-ground carbon pool," *Environ. Model. Softw.*, vol. 159, 2023, Art. no. 105580.
[3] Z. Fazakas, M. Nilsson, and H. Olsson, "Regional forest biomass and wood volume estimation using satellite data and ancillary data," *Agricultural Forest Meteorol.*, vol. 98, pp. 417–425, 1999.
[4] S. Condés and R. E. McRoberts, "Updating national forest inventory estimates of growing stock volume using hybrid inference," *Forest Ecol. Manage.*, vol. 400, pp. 48–57, 2017.
[5] A. Gogoi, J. Ahirwal, and U. K. Sahoo, "Evaluation of ecosystem carbon storage in major forest types of eastern Himalaya: Implications for carbon sink management," *J. Environ. Manage.*, vol. 302, 2022, Art. no. 113972.
[6] L. Chen et al., "Improved estimation of forest stand volume by the integration of GEDI LiDAR data and multi-sensor imagery in the Changbai mountains mixed forests ecoregion (CMMFE), Northeast China," *Int. J. Appl. Earth Observ. Geoinf.*, vol. 100, 2021, Art. no. 102326.
[7] F. Moradi, A. A. Darvishsefat, M. R. Pourrahmati, A. Deljouei, and S. A. Borz, "Estimating aboveground biomass in dense Hyrcanian forests by the use of Sentinel-2 data," *Forests*, vol. 13, 2022, Art. no. 104.
[8] D. Ehlers et al., "Mapping forest aboveground biomass using multisource remotely sensed data," *Remote Sens.*, vol. 14, 2022, Art. no. 1115.
[9] B. Brede et al., "Non-destructive estimation of individual tree biomass: Allometric models, terrestrial and UAV laser scanning," *Remote Sens. Environ.*, vol. 280, 2022, Art. no. 113180.
[10] L. Torre-Tojal, A. Bastarrika, A. Boyano, J. M. Lopez-Guede, and M. Graña, "Above-ground biomass estimation from LiDAR data using random forest algorithms," *J. Comput. Sci.*, vol. 58, 2022, Art. no. 101517.
[11] K. I. Paul et al., "Testing the generality of above-ground biomass allometry across plant functional types at the continent scale," *Glob. Change Biol.*, vol. 22, pp. 2106–2124, 2016.
[12] Z. Zhang, T. Wang, A. K. Skidmore, F. Cao, G. She, and L. Cao, "An improved area-based approach for estimating plot-level tree DBH from airborne LiDAR data," *Forest Ecosyst.*, vol. 10, 2023, Art. no. 100089.
[13] K. Liao, Y. Li, B. Zou, D. Li, and D. Lu, "Examining the role of UAV Lidar data in improving tree volume calculation accuracy," *Remote Sens.*, vol. 14, 2022, Art. no. 4410.
[14] X. Liang et al., "Close-range remote sensing of forests: The state of the art, challenges, and opportunities for systems and data acquisitions," *IEEE Geosci. Remote Sens. Mag.*, vol. 10, no. 3, pp. 32–71, Sep. 2022.
[15] S. Francini, G. D. Amico, E. Vangi, C. Borghi, and G. Chirici, "Integrating GEDI and Landsat: Spaceborne LiDAR and four decades of optical imagery for the analysis of forest disturbances and biomass changes in Italy," *Sensors*, vol. 22, 2022, Art. no. 2015.
[16] E. W. Mauya, J. Koskinen, K. Tegel, J. Hämäläinen, T. Kauranne, and N. Käyhkö, "Modelling and predicting the growing stock volume in small-scale plantation forests of Tanzania using multi-sensor image synergy," *Forests*, vol. 10, 2019, Art. no. 279.
[17] P. Kilpeläinen and T. Tokola, "Gain to be achieved from stand delineation in LANDSAT TM image-based estimates of stand volume," *Forest Ecol. Manage.*, vol. 124, pp. 105–111, 1999.
[18] A. Lausch, S. Erasmi, D. King, P. Magdon, and M. Heurich, "Understanding forest health with remote sensing—Part II: A review of approaches and data models," *Remote Sens.*, vol. 9, 2017, Art. no. 129.
[19] I. Chrysafis, G. Mallinis, M. Tsakiri, and P. Patias, "Evaluation of single-date and multi-seasonal spatial and spectral information of Sentinel-2 imagery to assess growing stock volume of a Mediterranean forest," *Int. J. Appl. Earth Observ. Geoinf.*, vol. 77, pp. 1–14, 2019.
[20] D. Lu, "The potential and challenge of remote sensing-based biomass estimation," *Int. J. Remote Sens.*, vol. 27, pp. 1297–1328, 2006.

[21] W. Huang, G. Sun, W. Ni, Z. Zhang, and R. Dubayah, "Sensitivity of multi-source SAR backscatter to changes in forest aboveground biomass," *Remote Sens.*, vol. 7, pp. 9587–9609, 2015.
[22] J. Hyyppä, H. Hyyppä, M. Inkinen, M. Engdahl, S. Linko, and Y. Zhu, "Accuracy comparison of various remote sensing data sources in the retrieval of forest stand attributes," *Forest Ecol. Manage.*, vol. 128, pp. 109–120, 2000.
[23] J. Long, H. Lin, G. Wang, H. Sun, and E. Yan, "Mapping growing stem volume of Chinese fir plantation using a saturation-based multivariate method and quad-polarimetric SAR images," *Remote Sens.*, vol. 11, 2019, Art. no. 1872.
[24] S. Jin et al., "Lidar sheds new light on plant phenomics for plant breeding and management: Recent advances and future prospects," *ISPRS J. Photogramm. Remote Sens.*, vol. 171, pp. 202–223, 2021.
[25] X. Liang et al., "Terrestrial laser scanning in forest inventories," *ISPRS J. Photogramm. Remote Sens.*, vol. 115, pp. 63–77, 2016.
[26] S. Puliti, S. Saarela, T. Gobakken, G. Ståhl, and E. Næsset, "Combining UAV and sentinel-2 auxiliary data for forest growing stock volume estimation through hierarchical model-based inference," *Remote Sens. Environ.*, vol. 204, pp. 485–497, 2018.
[27] K. Kronseder, U. Ballhorn, V. Böhm, and F. Siegert, "Above ground biomass estimation across forest types at different degradation levels in central Kalimantan using LiDAR data," *Int. J. Appl. Earth Observ. Geoinf.*, vol. 18, pp. 37–48, 2012.
[28] L. Guo, Y. Wu, L. Deng, P. Hou, J. Zhai, and Y. Chen, "A feature-level point cloud fusion method for timber volume of forest stands estimation," *Remote Sens.*, vol. 15, 2023, Art. no. 2995.
[29] J. G. Henning and P. J. Radtke, "Detailed stem measurements of standing trees from ground-based scanning lidar," *Forest Sci.*, vol. 52, pp. 67–80, 2006.
[30] K. Liu, X. Shen, L. Cao, G. Wang, and F. Cao, "Estimating forest structural attributes using UAV-LiDAR data in Ginkgo plantations," *ISPRS J. Photogramm. Remote Sens.*, vol. 146, pp. 465–482, 2018.
[31] Y. Jiao, D. Wang, X. Yao, S. Wang, T. Chi, and Y. Meng, "Forest emissions reduction assessment using optical satellite imagery and space LiDAR fusion for carbon stock estimation," *Remote Sens.*, vol. 15, 2023, Art. no. 1410.
[32] R. Dubayah et al., "The global ecosystem dynamics investigation: High-resolution laser ranging of the Earth's forests and topography," *Sci. Remote Sens.*, vol. 1, 2020, Art. no. 100002.
[33] T. Feng et al., "A systematic evaluation of multi-resolution ICESat-2 ATL08 terrain and canopy heights in boreal forests," *Remote Sens. Environ.*, vol. 291, 2023, Art. no. 113570.
[34] Y. Su et al., "A vegetation mapping strategy for conifer forests by combining airborne LiDAR data and aerial imagery," *Can. J. Remote Sens.*, vol. 42, pp. 1–15, 2016.
[35] L. Zhang, Z. Shao, J. Liu, and Q. Cheng, "Deep learning based retrieval of forest aboveground biomass from combined LiDAR and Landsat 8 data," *Remote Sens.*, vol. 11, 2019, Art. no. 1459.
[36] Q. Li, F. K. K. Wong, and T. Fung, "Mapping multi-layered mangroves from multispectral, hyperspectral, and LiDAR data," *Remote Sens. Environ.*, vol. 258, 2021, Art. no. 112403.
[37] T. Hu, Y. Sun, W. Jia, D. Li, M. Zou, and M. Zhang, "Study on the estimation of forest volume based on multi-source data," *Sensors*, vol. 21, 2021, Art. no. 7796.
[38] W. Li, Z. Niu, H. Chen, D. Li, M. Wu, and W. Zhao, "Remote estimation of canopy height and aboveground biomass of maize using high-resolution stereo images from a low-cost unmanned aerial vehicle system," *Ecol. Indicators*, vol. 67, pp. 637–648, 2016.
[39] C. T. D. Almeida et al., "Combining LiDAR and hyperspectral data for aboveground biomass modeling in the Brazilian Amazon using different regression algorithms," *Remote Sens. Environ.*, vol. 232, 2019, Art. no. 111323.
[40] M. Poorazimy, S. Shataee, R. E. McRoberts, and J. Mohammadi, "Integrating airborne laser scanning data, space-borne radar data and digital aerial imagery to estimate aboveground carbon stock in Hyrcanian forests, Iran," *Remote Sens. Environ.*, vol. 240, 2020, Art. no. 111669.
[41] X. Zhu, S. Nie, C. Wang, X. Xi, J. Lao, and D. Li, "Consistency analysis of forest height retrievals between GEDI and ICESat-2," *Remote Sens. Environ.*, vol. 281, 2022, Art. no. 113244.
[42] Q. Guo et al., "Lidar boosts 3D ecological observations and modelings: A review and perspective," *IEEE Geosci. Remote Sens. Mag.*, vol. 9, no. 1, pp. 232–257, Mar. 2021.
[43] F. Sarrus and J. F. Rameaux, "Application des sciences accessoires et principalement des mathématiques à la physiologie générale (rapport sur une mémoire adressé à l'académic royale de médecine, séance du 23 juillet 1839)," *Bull. Acad. Med.*, vol. 3, pp. 1094–1100, Jan. 1839.
[44] C. I. B. Wallis et al., "Remotely sensed carbon content: The role of tree composition and tree diversity," *Remote Sens. Environ.*, vol. 284, 2023, Art. no. 113333.
[45] P. B. Reich, M. G. Tjoelker, J. Machado, and J. Oleksyn, "Universal scaling of respiratory metabolism, size and nitrogen in plants," *Nature*, vol. 439, pp. 457–461, 2006.
[46] R. J. Brohman, L. D. Bryant, D. Tart, and C. K. Brewer, *Existing Vegetation Classification and Mapping Technical Guide*. Washington, DC, USA: Gen-Tech, 2005.
[47] S. Sun, Z. Li, X. Tian, Z. Gao, C. Wang, and C. Gu, "Forest canopy closure estimation in greater Khingan forest based on Gf-2 data," in *Proc. IEEE Int. Geosci. Remote Sens. Symp.*, 2019, pp. 6640–6643.
[48] K. Chang and B. Tsai, "The effect of DEM resolution on slope and aspect mapping," *Cartogr. Geographic Inf. Sci.*, vol. 18, pp. 69–77, 1991.
[49] Guangzhou Geo Optical Technology Co., *Si-scan 2.1 3D Point Cloud Scanning Software*. Guangzhou, China: FORO, 2015.
[50] *Binary Stand Volume Table for Larix Principis-Rupprechtii in North China*, Standard DB21/T 2275-2014, 2014.
[51] Q. Yang et al., "Allometry-based estimation of forest aboveground biomass combining LiDAR canopy height attributes and optical spectral indexes," *Forest Ecosyst.*, vol. 9, 2022, Art. no. 100059.
[52] J. W. Rouse, R. H. Haas, J. A. Schell, and D. W. Deering, "Monitoring vegetation systems in the great plains with ERTS," *NASA Special Pub.*, vol. 351, 1974, Art. no. 309.
[53] A. A. Gitelson, R. Stark, U. Grits, D. Rundquist, Y. Kaufman, and D. Derry, "Vegetation and soil lines in visible spectral space: A concept and technique for remote estimation of vegetation fraction," *Int. J. Remote Sens.*, vol. 23, pp. 2537–2562, 2010.
[54] A. Huete, K. Didan, T. Miura, E. P. Rodriguez, X. Gao, and L. G. Ferreira, "Overview of the radiometric and biophysical performance of the MODIS vegetation indices," *Remote Sens. Environ.*, vol. 83, pp. 195–213, 2002.
[55] H. Sun et al., "Optimizing kNN for mapping vegetation cover of arid and semi-arid areas using Landsat images," *Remote Sens.*, vol. 10, 2018, Art. no. 1248.
[56] J. N. Epiphanio and A. R. Huete, "Dependence of NDVI and SAVI on sun/sensor geometry and its effect on fAPAR relationships in Alfalfa," *Remote Sens. Environ.*, vol. 51, pp. 351–360, 1995.
[57] S. Y. Chang, H.-C. Wu, Y.-C. Kuan, and Y. Wu, "Tensor Levenberg-Marquardt algorithm for multi-relational traffic prediction," *IEEE Trans. Veh. Technol.*, *IEEE Trans. Veh. Technol.*, vol. 72, pp. 11275–11290, 2023.
[58] N. C. Coops et al., "Modelling lidar-derived estimates of forest attributes over space and time: A review of approaches and future trends," *Remote Sens. Environ.*, vol. 260, 2021, Art. no. 112477.
[59] T. Jucker et al., "Allometric equations for integrating remote sensing imagery into forest monitoring programmes," *Glob. Change Biol.*, vol. 23, pp. 177–190, 2017.
[60] J. Kalliovirta and T. Tokola, "Functions for estimating stem diameter and tree age using tree height, crown width and existing stand database information," *Silva Fennica*, vol. 39, 2005, Art. no. 250254.
[61] D. Panagiotidis, A. Abdollahnejad, and M. Slavík, "3D point cloud fusion from UAV and TLS to assess temperate managed forest structures," *Int. J. Appl. Earth Observ. Geoinf.*, vol. 112, 2022, Art. no. 102917.
[62] L. Terryn et al., "Quantifying tropical forest structure through terrestrial and UAV laser scanning fusion in Australian rainforests," *Remote Sens. Environ.*, vol. 271, 2022, Art. no. 112912.
[63] L. Li, Q. Guo, S. Tao, M. Kelly, and G. Xu, "LiDAR with multi-temporal MODIS provide a means to upscale predictions of forest biomass," *ISPRS J. Photogramm. Remote Sens.*, vol. 102, pp. 198–208, 2015.
[64] T. Ma et al., "A novel vegetation index approach using sentinel-2 data and random forest algorithm for estimating forest stock volume in the Helan mountains, Ningxia, China," *Remote Sens.*, vol. 15, 2023, Art. no. 1853.

Yanjie Wu received the B.S. degree in remote sensing science and technology from Shandong Normal University, Jinan, China, in 2021. She is currently working toward the M.S. degree in cartography and geographic information system with Capital Normal University, Beijing, China.

Her research interests include UAV remote sensing, LiDAR, and its application in ecological research.

Zhihui Mao received the B.S. degree in remote sensing science and technology and the M.S. degree in map cartography and geographic information engineering in 2016 and 2019, respectively, from Capital Normal University, Beijing, China, where she is currently working toward the Ph.D. degree in cartography and geographic information system.

Her research interests include UAV remote sensing, LiDAR, and its application in ecological research.

Lijie Guo received the B.S. degree in geomatics engineering from Shangqiu Normal University, Shangqiu, China, in 2019. She is currently working toward the M.S. and Ph.D. degrees in cartography and geographic information system with Capital Normal University, Beijing, China.

Her research interests include remote sensing image processing and application and UAV forestry remote sensing.

Chenrui Li received the B.S. degree in land resource management from Shandong Agricultural University, Tai'an, China, in 2021. She is currently working toward the M.S. degree in cartography and geographic information system with Capital Normal University, Beijing, China.

Her research interests include UAV remote sensing and ocean remote sensing.

Lei Deng received the B.S. degree in cartography from Wuhan University, Wuhan, China, in 1998, and the Ph.D. degree in geography from Beijing Normal University, Beijing, China, in 2009.

He is currently a Professor with the School of Resources, Environment, and Tourism, Capital Normal University, Beijing, China. His research interests include UAV remote sensing, data fusion and artificial intelligence, remote sensing, and GIS applications.